



Quantitative multi-omics analysis of the effects of mitochondrial dysfunction on lipid metabolism in *Saccharomyces cerevisiae*

Xiaopeng Guo^{1,2} · Miaomiao Zhang^{1,2,3} · Yue Gao^{1,2} · Guozhen Cao⁴ · Dong Lu^{1,3} · Wenjian Li^{1,3}

Received: 26 September 2019 / Revised: 8 November 2019 / Accepted: 15 November 2019 / Published online: 12 December 2019
© Springer-Verlag GmbH Germany, part of Springer Nature 2019

Abstract

In this study, combined genome, transcriptome, and metabolome analysis was performed for eight *Saccharomyces cerevisiae* mitochondrial respiration-deficient mutants. Each mutant exhibited a unique nuclear genome mutation pattern; the nuclear genome mutations, and thus potentially affected genes and metabolic pathways, showed a co-occurrence frequency of ≤ 3 among the eight mutants. For example, only a lipid metabolism-related pathway was likely to be affected by the nuclear genome mutations in one of the mutants. However, large deletions in the mitochondrial genome were the shared characteristic among the eight mutants. At the transcriptomic level, lipid metabolism was the most significantly enriched Kyoto Encyclopaedia of Genes and Genomes (KEGG) pathway for differentially expressed genes (DEGs) co-occurring in both ≥ 4 and ≥ 5 mutants. Any identified DEG enriched in lipid metabolism showed the same up-/down-regulated pattern among nearly all eight mutants. Further, 126 differentially expressed lipid species (DELS) were identified, which also showed the same up-/down-regulated pattern among nearly all investigated mutants. It was conservatively demonstrated that the similar change pattern of lipid metabolism in the entire investigated mutant population was attributed to mitochondrial dysfunction. The change spectrum of lipid species was presented, suggesting that the number and change degree of up-regulated lipid species were higher than those of down-regulated lipid species. Additionally, energy storage lipids increased in content and plasma-membrane phospholipid compositions varied in the relative proposition. The results for the genome, transcriptome, and lipidome were mutually validated, which provides quantitative data revealing the roles of mitochondria from a global cellular perspective.

Keywords Multi-omics analysis · Mitochondria · Lipid metabolism · Respiration-deficient mutant · *Saccharomyces cerevisiae*

Xiaopeng Guo and Miaomiao Zhang contributed equally to this work and should be considered co-first authors.

Electronic supplementary material The online version of this article (<https://doi.org/10.1007/s00253-019-10260-z>) contains supplementary material, which is available to authorized users.

✉ Dong Lu
ld@impcas.ac.cn

¹ Institute of Modern Physics, Chinese Academy of Sciences, Lanzhou 730000, China

² College of Life Science, University of Chinese Academy of Sciences, Beijing 100049, China

³ Gansu Key Laboratory of Microbial Resources Exploitation and Application, Lanzhou 730000, China

⁴ University of Science and Technology of China, Hefei 230026, China

Introduction

As an important organelle in eukaryotic cells, mitochondria play a pivotal role in cellular activity. Mitochondria provide energy for normal cell activities and thus is referred to as cell energy factory (Frazier et al. 2019); mitochondria are the centres of cellular material metabolism (Lozoya et al. 2018; Schell et al. 2017) and function as important nodes in cell signalling, such as activating longevity and mediating apoptosis (Gureev et al. 2019; Zhao et al. 2016). However, mitochondrial DNA (mtDNA) is not encapsulated by nucleosomes (Dobson et al. 2000) and mitochondria are important sites for generating reactive oxygen species (ROS) during cellular emergency (Chouchani et al. 2014), making mtDNA susceptible to ROS attack. Additionally, many DNA repair systems that repair nuclear DNA damage are not active in mitochondria (Van Houten et al. 2016). Thus, mtDNA is more frequently damaged and mutated than nuclear DNA. Studies have

shown that the frequency of mtDNA mutations in *Saccharomyces cerevisiae* is approximately 10-fold that of nuclear DNA mutations (Lynch et al. 2008). As basic mitochondrial functions depend on the encoded products of mitochondrial genes (Yan et al. 2019), mtDNA mutations often lead to functional defects, resulting in mitochondrial diseases (Ryzhkova et al. 2018). Therefore, the importance and vulnerability of mitochondrial function reinforce the great significance of studies on mitochondria.

Mitochondria have always been a significantly important subject of study in the field of life sciences. On the one hand, a large amount of basic data that substantiate previous conclusions have been obtained. For example, mtDNA mutational hotspots, which are closely related to disease and ageing, have been extensively examined (Hirose et al. 2016; Niemann et al. 2017; Spangenberg et al. 2019), mitochondrial protein maps have been accurately drawn (Calvo et al. 2016; Sickmann et al. 2003), and the localizations of many important signalling molecules in mitochondria have been identified (Calvo et al. 2016). On the other hand, new findings about mitochondria are constantly being reported. Recently, the relationship between mitochondrial metabolism and epigenetic modification of chromatin gained attention (Matilainen et al. 2017; Mayorga et al. 2019). Additionally, studies by Benador et al. (2018) demonstrated that a specific set of mitochondria in cells can adsorb fat droplets and provide energy to synthesize and store lipid molecules. Sun et al. (2017) found that the mitochondrial “pseudomembrane potential” maintained by exogenous positive charges can induce autophagy in cells.

Although many specific signalling pathways, metabolic pathways, and metabolites affected by mitochondria have been characterized, quantitative data are scarce. Additionally, data from distinctive studies are lacking crosswise comparison. Thus, studies are needed to relatively or absolutely quantify metabolic pathways and metabolites affected by mitochondria at the global cellular level. Mitochondrial mutants are the preferred material for these studies; however, it is difficult for researchers to obtain important mitochondrial mutants for large-scale functional studies. First, the loss of important mitochondrial genes is often accompanied by inactivation of mammalian cells. Second, the current commercial gene editing technology of clustered regularly interspaced short palindromic repeats-associated protein 9 (CRISPR-Cas9) has not been widely applied to mtDNA editing. The main limitation is that the CRISPR-cas9 system cannot be simply and efficiently transferred into mitochondria and the mitochondrial relatively narrow space is not conducive to operation of the CRISPR-cas9 system (Bacman et al. 2018; Gammage et al. 2018). Moreover, human cells contain thousands of copies of mitochondria, with dozens of copies in *S. cerevisiae* (Solieri 2010; St John 2016). Thus, genetic manipulation of mtDNA involves a relative proportion of edited

mtDNA compared to normal mtDNA, making the analyses complex.

Heavy ion beam (HIB) irradiation is a typical ionising radiation (Feng et al. 2006). Compared with traditional mutagenesis methods, HIB irradiation mutagenesis possesses the advantages of high mutation rate, large mutation spectrum, and significant mutant traits (Feng et al. 2006; Du et al. 2017; Guo et al. 2019a). It has been widely used to develop advantageous mutants with great application potential and research value (Du et al. 2014; Li et al. 2018; Luo et al. 2016; Zhang et al. 2018a). Particularly, HIB irradiation mutagenesis showed an excellent performance in the establishment of a mutant library (Du et al. 2017; Guo et al. 2019a). In this study, a group of HIB irradiation-induced *S. cerevisiae* mitochondrial respiration-deficient mutants were selected as the research material. As a facultative anaerobic eukaryote, *S. cerevisiae* can grow at a low rate by anaerobic respiration when mitochondrial function is severely impaired. This enabled us to obtain detailed information on the effects of impaired mitochondrial function on cells. Multi-omics studies were conducted at the mutant population level. Genomic, transcriptomic, and metabolomic analyses were combined to ensure high throughput and reliability. The research methods and strategies focus on measuring the extent to which metabolic pathways are most dominated by mitochondria and the ultimate phenotypic effects of this dominance.

Materials and methods

Strain culture and mitochondrial respiration ability measurement

S. cerevisiae BY4743 (American Type Culture Collection (ATCC), Manassas, VA, USA; collection number: ATCC4040005) is amphidiploid (MATa/ α , budding) and was derived from type strain S288c. The strains used in this study were a wild-type *S. cerevisiae* BY4743 strain and eight genetically stable respiration-deficient mutants of BY4743. These mutants (RD-1, RD-2, RD-3, RD-4, RD-5, RD-6, RD-7, and RD-8) were previously screened following moderate-energy carbon ion beam irradiation (Guo et al. 2019a). Carbon ion beam irradiation was generated by accelerating $^{12}\text{C}^{6+}$ to approaching light speed using the Heavy Ion Research Facility in Lanzhou (HIRFL) at the Institute of Modern Physics at the Chinese Academy of Sciences. The average dose rate was about 40 Gy min^{-1} . As it reached the sample surface, the retained energy was approximately 76.37 MeV u^{-1} , and the expected range in water was about 16 mm. More details on mutagenesis, screening, and mutant evaluation were described in our previous report (Guo et al. 2019a). Each strain was inoculated into yeast extract peptone dextrose medium (YEPD) at a ratio of 1:100, and then

incubated in a shaker (200 rpm) at 30 °C. In addition, triphenyl tetrazolium chloride (TTC) medium was used to detect the weak mitochondrial respiration of each mutant. The principle, protocols, and validity of the TTC method have been described previously (Guo et al. 2019a; Mao et al. 2009).

Genomic analysis

The genome sequences of nine strains involved in this study were obtained from our previous work (Guo et al. 2019a). Specific mutations in each mutant strain were identified. In this study, the BAM format of sequence files were sorted, indexed, and then loaded into Integrative Genomics Viewer (<http://software.broadinstitute.org/software/igv/>, v.2.3). Next, the mitochondrial genomes of the nine strains were visually presented in a X-Y scheme. The mutation sites in the nuclear genomes of eight mutants were drawn using Circos software based on Perl programming language (Krzywinski et al. 2009).

RNA-seq

The *S. cerevisiae* cells ($\sim 10^8$) were collected at logarithmic phase and then snap-frozen in liquid nitrogen. Total RNA extraction, library construction, clustering and sequencing, data cleaning, quality control, transcript assembly, and fragments per kilobase of exon per million fragments mapped (FPKM) calculation were performed as described previously (Guo et al. 2019b). The transcripts were picked and searched in the genome browser of BioCyc database to identify the specific genes included in the transcripts. The genes with a fold change (FC) of FPKM > 1.5 or < 0.67 and corresponding p value < 0.05 were identified as differentially expressed genes (DEGs) between the wild-type and mutant strains. A portion of genes from DEGs were subjected to reverse transcriptase quantitative polymerase chain reaction (RT-qPCR) to verify the results of RNA sequencing (RNA-seq). The detailed manipulations were identical to the protocols introduced in our previous study (Guo et al. 2019b). The primer sequences are shown in Supplemental Table S1.

GO and KEGG analysis

All genes in the reference genome were annotated based on Goatools (<https://github.com/tanghaibao/Goatools>) and KOBAS (Wu et al. 2006). Next, the gene sets obtained from genomic or transcriptomic analysis were enriched with different gene ontology (GO) or Kyoto Encyclopaedia of Genes and Genomes (KEGG) terms. The enrichment factor and enrichment significance (q value) were calculated based on R programming language.

Lipidome detection

The centrifugally harvested cells at logarithmic phase were snap-frozen in liquid nitrogen after washing twice with phosphate-buffered saline. The cell precipitates were thawed at 4 °C. Next, the same weight of the cell precipitates of the wild-type strain, randomly selected five mutant strains, and quality control (QC) sample were weighed. The QC sample consists of the same weight of cell precipitates from the wild-type strain and five mutant strains. The seven groups of cell precipitates were prepared to extract lipids after resuspension in phosphate-buffered saline. Six repeats were used for each group.

Total lipids were extracted as described previously (Ejsing et al. 2009). Ultra-high-performance liquid chromatography-electrospray ionization mass spectrometry (UHPLC-ESI-MS) analysis was carried out as follows. First, the extracted lipid was reconstituted in 200 μ L of isopropanol solution and vortexed, and the insoluble matter was removed by centrifugation. The sample was then separated by UHPLC and ion trap mass spectrometry (ITMS) (Q Exactive Plus, Thermo Scientific, Waltham, MA, USA). Data were collected using ESI in positive and negative ion modes, respectively. The raw data from UHPLC-ITMS was manipulated based on LipidSearch™ software version 4.1 (Thermo Scientific) for peak identification, lipid identification (secondary identification), peak extraction, peak alignment, and lipid quantification. The LC-MS conditions and data procurement parameters conformed to the established pattern in our previous study (Zhang et al. 2018b).

Data reliability

The average read coverage was $\sim 200\times$ for the whole-genome sequence data. RNA-seq was repeated at least three times. The FPKM and DEGs were determined by three repeated tests showing the closest transcriptional pattern. RT-qPCR was performed in at least triplicate and repeated three times independently. Lipidomic detection was performed using six independent repeats.

Availability of supporting data

The raw sequence data obtained by genomic sequencing and transcriptomic sequencing have been deposited in the Genome Sequence Archive in the BIG Data Center, Beijing Institute of Genomics, Chinese Academy of Sciences, respectively, under the accession numbers CRA001107 and CRA001812, which are publicly accessible at <http://bigd.big.ac.cn/gsa>.

Results

Large structural variations co-presented in the mitochondrial genomes of the eight mitochondrial respiration-deficient mutants

The TTC method was used to qualitatively show the mitochondrial respiration intensity in each mutant (Fig. 1a). The lawns of the mutant strains appeared white when incubated in TTC medium, suggesting that the mutants did not effectively convert TTC to red triphenylformazan as in the wild-type strain, which was a sign of severe dysfunction in the mitochondrial electron transport respiratory chain (Guo et al. 2019a; Mao et al. 2009). The extremely weak mitochondrial respiration intensity compared to the wild-type strain indicated the phenotypic commonality of the eight mutants.

At the molecular level, the eight mutants were found to have very large deletions in the mitochondrial genomic DNA (Guo et al. 2019a). Moreover, these regions contained important mitochondrial coding genes. For example, *COX1*, *COB*, and *COX2* were deleted in seven

mutants, while *COX3* was deleted in five (Fig. 1b). These mitochondrial genes code for important components of the electron transport respiratory chain. Additionally, we investigated nuclear genes that are likely to decrease mitochondrial respiratory function due to the nuclear genome mutations. A nuclear genome mutation may alter biological functions in one of the following situations. First, the mutation was annotated to the class of non-synonymous coding, frame shift, or codon change plus codon insertion. Second, the mutation located at 1–2000 base pairs (bp) upstream of the transcription start site and the transcriptional level of potentially affected genes was changed. To reduce the false-negative rate of judgment, $p < 0.2$ was selected as the significant difference threshold to identify potentially effected genes with altered transcript abundance. Finally, three nuclear genes likely to decrease mitochondrial respiratory function were identified in three respective mutants (Supplemental Table S2). Thus, the mitochondrial respiratory dysfunctions in only ≤ 3 mutants may have been contributed by functional variances of mitochondrial respiration-related nuclear genes. Based on comprehensive analysis, the large

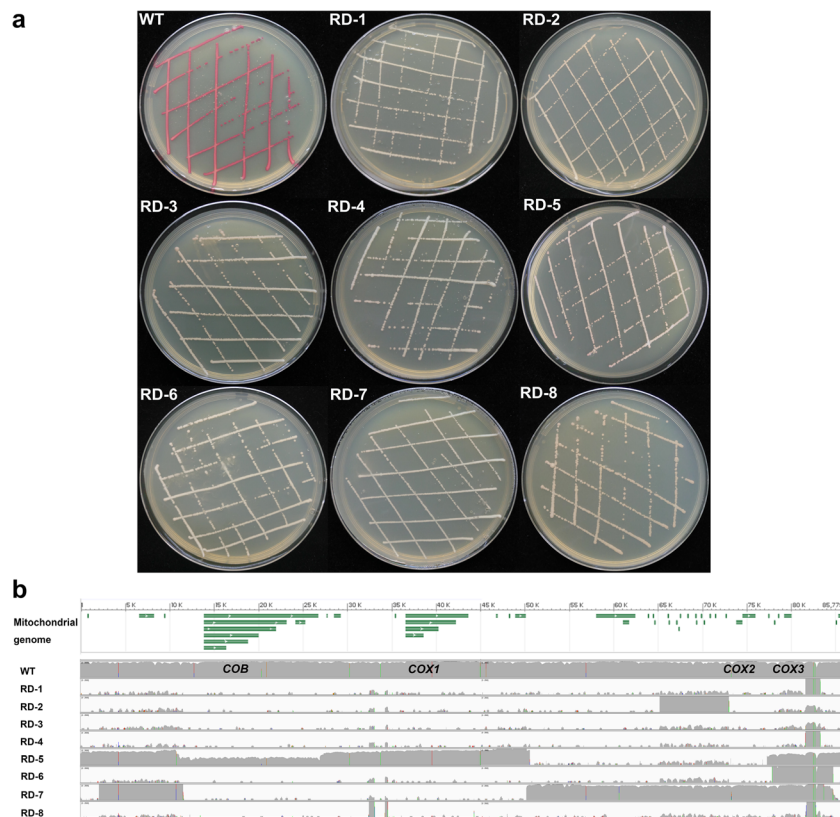


Fig. 1 Comparison of mitochondrial respiration intensity and mitochondrial genomes between mutant and wild-type strains. After 3 h of incubation in TTC medium, the lawns of the wild-type strain stained red, while the mutant lawns remained white (a), indicating that the mutant respiratory function was severely impaired, so that few [H] (reduced hydrogen) in the electron-transferred respiratory chain were not enough

to reduce the TTC to produce red triphenylformazan. Under the same sequencing system, the mitochondrial genome of the wild-type strain was covered by sufficient reads with an average read coverage of > 2000 . However, a large range of regions in the mitochondrial genome of each mutant showed nearly no read coverage, and these regions contained important mitochondrial genes (b)

structural variation (SV) in the mitochondrial genome was the shared characteristic of all investigated mutants and the main cause of mitochondrial dysfunction. The mitochondrial dysfunctions in ≥ 5 mutants were caused by large SVs in the mitochondrial genomes.

Low co-occurrence frequency (≤ 3) among the eight mutants for nuclear genome variations

In the nuclear genome, the average number of mutation sites for each mutant was ~ 14 (Guo et al. 2019a). The distribution patterns between mutants were distinct (Fig.

2a). Most mutation sites were unique to the nuclear genome of any one mutant. Only four mutation sites were shared by any two mutants (Fig. 2a). The genes potentially affected by nuclear genome mutations were identified as described above. Mutations in both coding regions and promoter regions were considered. Whether mutation in the promoter region was likely to change the biological function, was judged by the variance in mRNA expression abundance of the corresponding gene. Finally, an average of 11 nuclear genes were regarded as potentially affected by nuclear genome mutations in each mutant, with only a few very small intersections (Fig. 2b). *YHR201C* was co-

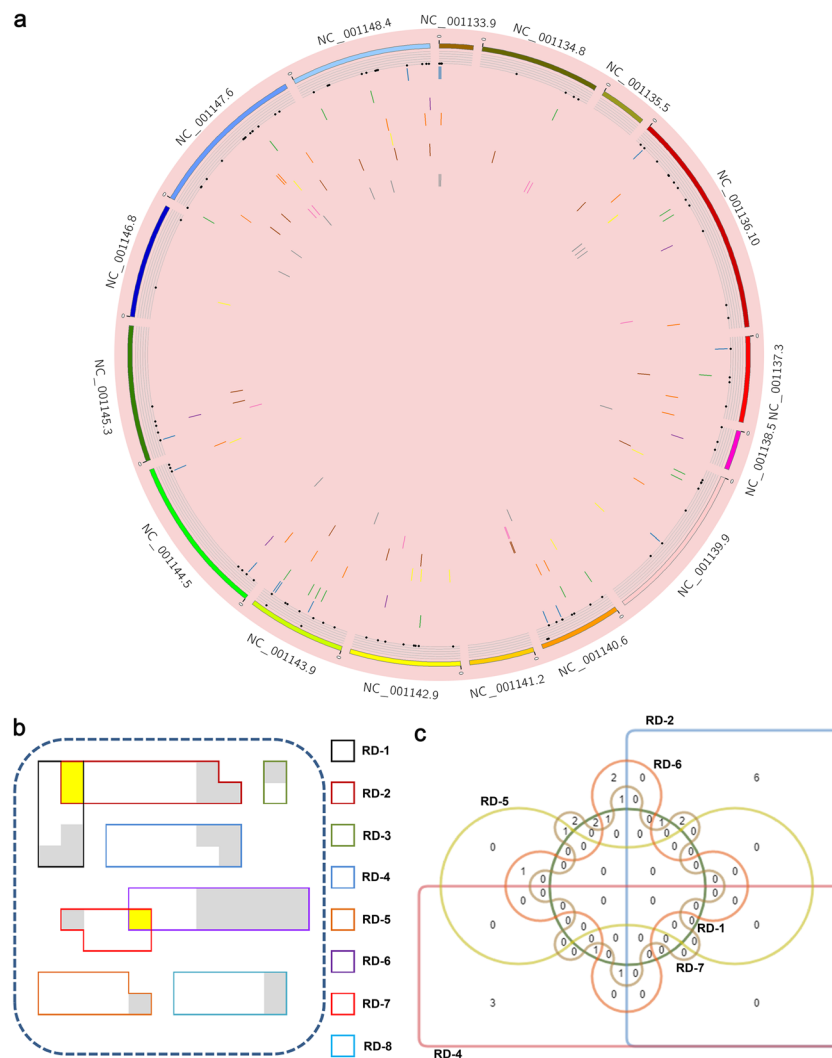


Fig. 2 Very low co-occurrence frequency of nuclear genome mutation (≤ 3 mutants) in the mutant population. **a** Scatters in the first circle represents the accumulative mutation frequency of the eight mutants at a nuclear genome position, in which near the centre and far from the centre represented values of 1 and 2, respectively; the distribution of mutation sites in the nuclear genomes of eight mutants (from RD-1–8) was displayed in the highlighted form in the circles 2–8 of the Circos diagram. **b** Potentially affected genes by nuclear genome mutations and their intersections in

eight mutants. The area of the legend represents a gene, while the shaded part indicates genes potentially affected by mutations located in the promoter regions. **c** Annotated KEGG pathway for genes potentially affected by the nuclear genome mutations and their intersection in eight mutants. The maximum co-occurrence frequency of the nuclear genome mutation sites, its potentially affected genes, and thus the possibly altered KEGG pathways in the eight mutants were 2, 2, and 3, respectively

identified in the RD-6 and RD-7 strains, while *YKL068W* and *YKR079C* were co-identified in the RD-1 and RD-2 strains. Therefore, the maximum co-occurrence frequency of genes affected by the nuclear genome mutations was two among the eight mutants (Fig. 2b). The identified genes were evaluated by KEGG pathway annotation. A total of 24 KEGG pathways were annotated for these genes potentially affected by the nuclear genome mutations (Table 1); fifteen of them existed only in one of the mutants (Table 1 and Fig. 2c). For example, only a lipid metabolism-related pathway (steroid biosynthesis) was found in RD-1 (Table 1). Additionally, eight of them showed a co-occurrence frequency of two; purine metabolism co-existed in the RD-4, RD-6, and RD-7 mutants, which hold the highest co-occurrence frequency of three among the eight mutants (Table 1 and Fig. 2c).

DEG distribution pattern among the eight mutants

The distribution pattern of all DEGs among the eight mutants is shown in Fig. 3. The average number of DEGs was 775 in

each mutant (Fig. 3a). A total of 1548 genes were down-regulated and 1296 genes were up-regulated in the investigated mutant population (Fig. 3b–d). As the co-occurrence frequency increased, the number of DEGs decreased rapidly, both for up-regulated and down-regulated genes (Fig. 3b–d). A total of 506 DEGs showed a co-occurrence frequency of ≥ 4 , of which 349 were down-regulated and 157 were up-regulated (Fig. 3b–d). Sixteen, 51, 69, 134, and 236 DEGs co-occurred in any of the 8, 7, 6, 5, and 4 mutants, respectively (Fig. 3b–d).

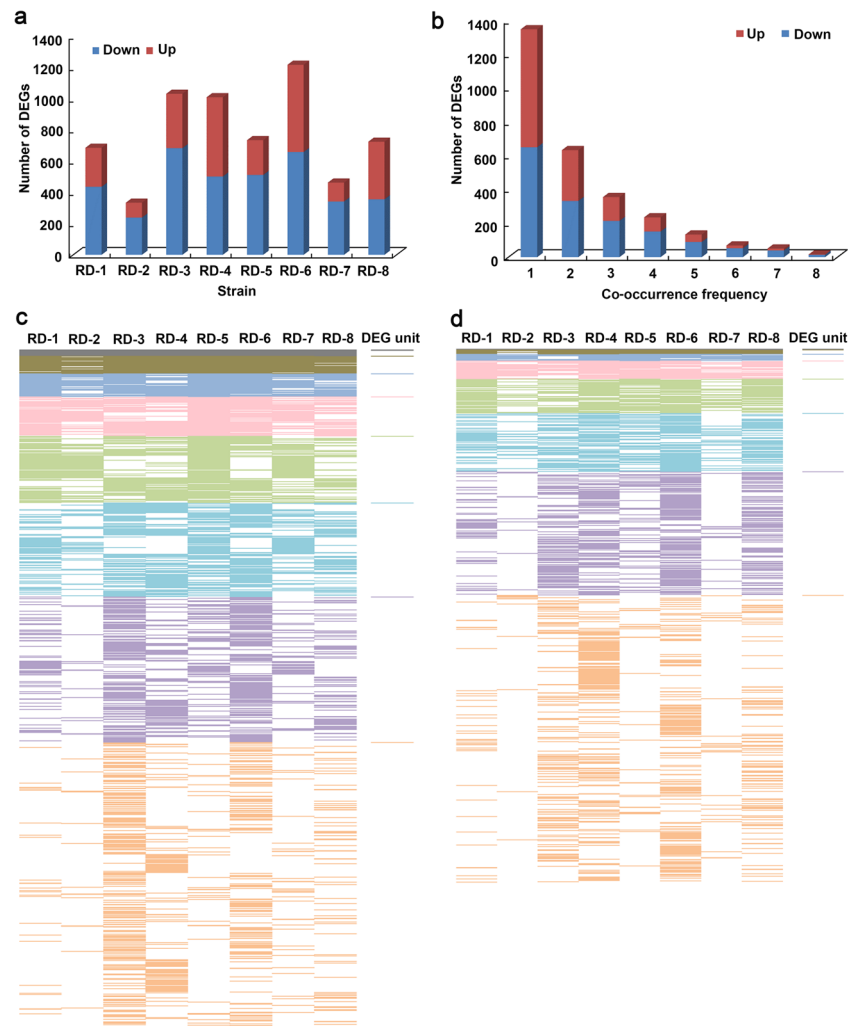
KEGG enrichment analysis of DEGs with co-occurrence frequencies ≥ 4 and ≥ 5 among the eight mutants

For mutations in the nuclear genomes, the mutation sites, genes potentially affected by the mutations, or possibly altered KEGG pathways showed a maximum co-occurrence frequency of three among the eight mutants (Fig. 2). However, the phenotype of mitochondrial respiratory dysfunction and the large deletions in the mitochondrial genome co-occurred in all investigated mutants (Fig. 1). Based on this genetic

Table 1 Potentially affected KEGG pathways by mutations in the nuclear genome among the mutant population

KEGG pathways	Strains with specific potentially affected KEGG pathways by the nuclear genome mutations	Co-occurrence frequencies of specific potentially affected KEGG pathways by the nuclear genome mutations among the mutant population
Amino sugar and nucleotide sugar metabolism	RD-2	1
Arginine and proline metabolism	RD-1	1
Base excision repair	RD-4	1
Carbon metabolism	RD-2; RD-7	2
DNA replication	RD-4	1
Endocytosis	RD-6	1
Galactose metabolism	RD-2	1
Glyoxylate and dicarboxylate metabolism	RD-2; RD-7	2
mRNA surveillance pathway	RD-5; RD-6	2
N-Glycan biosynthesis	RD-6; RD-7	2
Nicotinate and nicotinamide metabolism	RD-7	1
Nucleotide excision repair	RD-1; RD-4	2
Pentose and glucuronate interconversions	RD-2	1
Peroxisome	RD-7	1
Protein processing in endoplasmic reticulum	RD-1; RD-6	2
Purine metabolism	RD-4; RD-6; RD-7	3
Pyrimidine metabolism	RD-4	1
Ribosome	RD-2	1
Ribosome biogenesis in eukaryotes	RD-5; RD-7	2
RNA transport	RD-1; RD-2	2
Spliceosome	RD-6	1
Starch and sucrose metabolism	RD-2	1
Steroid biosynthesis	RD-1	1
Sulfur relay system	RD-2	1

Fig. 3 Distribution pattern of the DEGs among the eight mutants. The DEG number of each mutant (vs. wild-type strain) are shown in **a** DEG number corresponding to a specific co-occurrence frequency among eight mutants are shown in **b**. **c**, **d** Up-regulated and down-regulated DEGs, respectively; the eight colors (from top to bottom) represent different co-occurrence frequencies (from 8 to 1); the thickness of the legend line represents a DEG



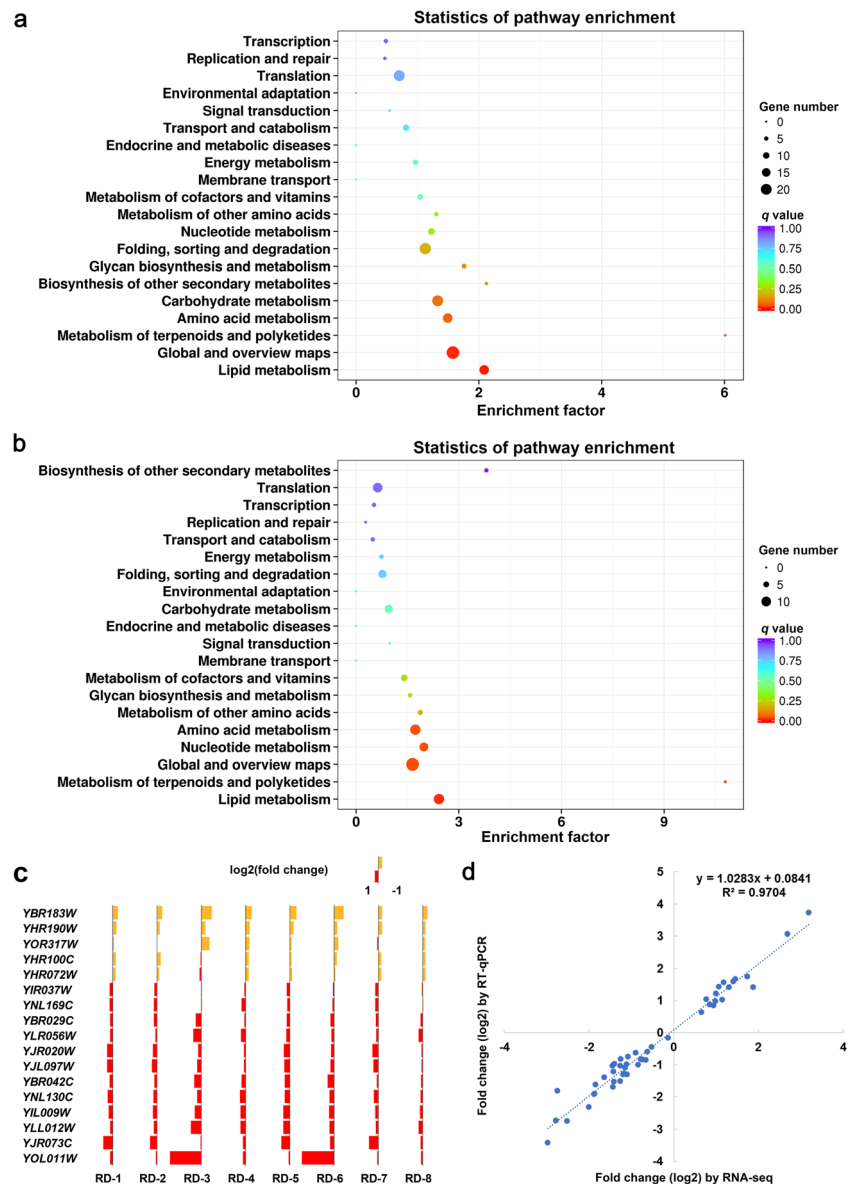
background, DEGs with a co-occurrence frequency > 3 among the eight respiratory-deficient mutants were selected for analysis to conservatively identify the most significant metabolic pathways affected by mitochondrial dysfunction and exclude the interference caused by unrelated nuclear genes.

The DEGs with co-occurrence frequencies ≥ 4 and ≥ 5 were subjected to their respective KEGG pathway enrichment analysis (Fig. 4a, b). All 20 secondary enrichment terms were selected because the biological pathways related to mitochondria are very extensive, making it difficult to obtain a few relatively prominent KEGG enrichment terms at the third-class level. The q value and enrichment factor were used as the first and second indicators for judging the significance of enrichment, respectively. Lipid metabolism showed the lowest q value for DEGs with co-occurrence frequencies of both ≥ 4 and ≥ 5 . In addition, the enrichment factor of lipid metabolism was in the top three among all enriched terms (Fig. 4a, b). Based on the overall consideration of the q value and enrichment factor, lipid metabolism was the most significant enrichment term.

Similar expression patterns of the identified lipid metabolism-related DEGs among nearly all eight mutants at the transcriptional level

Based on KEGG pathway enrichment of the DEGs with a co-occurrence frequency ≥ 4 among the eight mutants, genes enriched in the term of lipid metabolism were collected. In Fig. 4c, the FC in the expression abundance of these genes in the eight mutants (vs. wild-type strain) was enumerated. All these lipid metabolism-related genes showed the same up/down-regulated expression pattern among nearly all eight mutants at the transcriptional level (Fig. 4c). As the annotation results on nuclear genome mutations suggests that only a lipid metabolism-related pathway was potentially affected in one of the mutants (Table 1), the similar change pattern of the identified lipid metabolism-related DEGs among the eight mutants can be conservatively attributed to the population commonality of mitochondrial dysfunction. Additionally, RT-qPCR was performed to determine the FC in the expression abundance of some lipid-related genes (*YBR183W*, *YHR190W*, *YOL011W*,

Fig. 4 KEGG pathway enrichment results for DEGs with co-occurrence frequencies ≥ 4 and ≥ 5 among the eight mutants. Considering the q value and enrichment factor, lipid metabolism was the most significantly enriched KEGG term for DEGs with co-occurrence frequencies of both ≥ 4 (a) and ≥ 5 (b). Each DEG enriched in lipid metabolism showed the same up- or down-regulated pattern among nearly all eight mutants (c). The randomly selected RNA-seq results and corresponding RT-qPCR results and corresponding RT-qPCR results were linearly fitted. The determination coefficient was approximately 0.9, indicating that the RNA-seq results agreed well with RT-qPCR results (d)



YJR073C, *YLL012W*, and *YIL009W*) in the eight mutants (vs. wild-type strain) (Supplemental Table S3). The transcriptome and RT-qPCR results were evaluated by linear correlation analysis (Fig. 4d). The coefficient of determination was ~ 0.9 , supporting the reliability of transcriptomic analysis results.

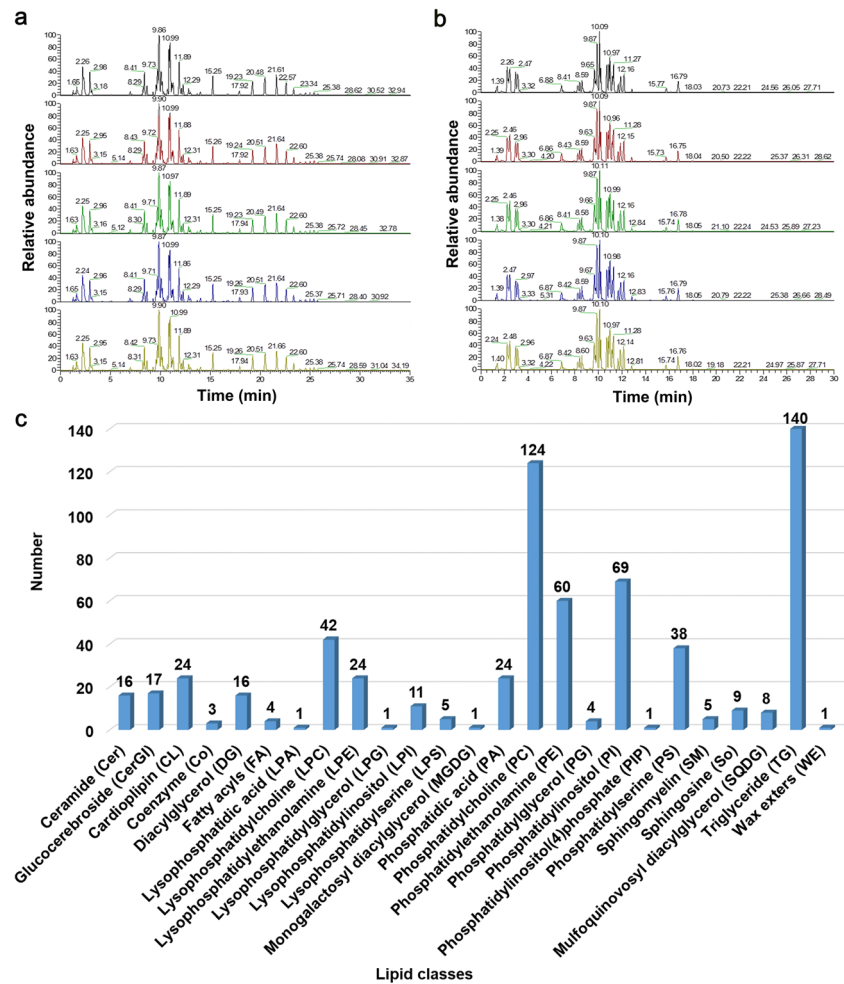
The third-class metabolic pathways that may be affected by the identified lipid metabolism-related DEGs were analyzed (Fig. 5a). Fatty acids are one of the simplest fats and a component of many complex lipids. Both the fatty acid synthesis and degradation pathways contained up-regulated as well as down-regulated DEGs. Additionally, the glycerophospholipid metabolism pathway contained the most DEGs (Fig. 5a). Thus, the potentially affected catalytic enzymes by the identified lipid metabolism-related DEGs were presented in the glycerophospholipid metabolism network (Fig. 5b). It can be

seen that catalytic enzymes that may be affected by the DEGs were dispersed throughout the metabolic network; crosstalk was common among various glycerophospholipids. Taking phosphatidylethanolamine (PE) as an example, almost all of the DEGs affecting the catalytic enzymes in the metabolic network located upstream or downstream of PE metabolism (Fig. 5b). Therefore, it was challenging to infer the change pattern (up-regulated or down-regulated) of a certain lipid class based on these DEGs.

Similar change patterns of the identified differentially expressed lipid species among nearly all investigated mutants revealed by lipidomic analysis

Five randomly selected mutants and the wild-type strain were evaluated using lipidomic analysis. A total of 36 lipid extracts

Fig. 6 Stable and reliable UHPLC-ESI-MS system and identified lipid classes. **a, b** The base peak of UHPLC-ESI-MS for five QC samples in positive ion and negative ion modes, respectively. The response intensity and retention time of each chromatographic peak exhibited good reproducibility, indicating the high stability and reliability of the analytical system. **c** Identified lipid classes and number of lipid species in each lipid class



with great biological significance, the variable importance in projection (VIP) > 1 was selected as one of the screening thresholds, which was obtained according to the valid OPLS-DA model, and was used to measure the influence intensity and explanatory ability of each lipid expression pattern on the classification and discrimination of each group of samples. In addition, the screening threshold of FC was adjusted to > 1.5 or < 0.67 to relieve the strictness of screening conditions. Finally, the DELS were judged by a *p* value < 0.05, FC > 1.5 or < 0.67, and VIP > 1. Based on this, a total of 126 DELS were collected and the relative FCs of these lipid species in the examined mutants (vs. wild-type strain) was enumerated (Fig. 8b). At the metabolic level, all DELS showed the same pattern of up-/down-regulation among nearly all investigated mutants, which is consistent with the transcriptional data and can be also conservatively attributed to the population commonality of mitochondrial dysfunction.

Up-regulated lipid classes contained TG (32 lipid species), PC (15 lipid species), lysophosphatidylcholine (LPC; 10 lipid species), lysophosphatidylethanolamine (LPE; 7 lipid species), PI (5 lipid species), DG (4 lipid species), lysophosphatidylinositol (LPI; 2 lipid species), PA (2

lipid species), PE (1 lipid species), PS (1 lipid species), and SQDG (1 lipid species) (Fig. 8b). Down-regulated lipid classes contained PE (18 lipid species), PC (14 lipid species), PS (8 lipid species), PI (3 lipid species), LPE (1 lipid species), LPI (1 lipid species), and lysophosphatidylserine (LPS; 1 lipid species) (Fig. 8b). The number of up-regulated lipid species was 1.74-fold higher than that of down-regulated lipid species (Fig. 8b, c). The average $\log_2(\text{FC})$ of all identified DELS in all detected mutants was 0.54 (Fig. 8b, d). The average $\log_2(\text{FC})$ of up-regulated lipid species in all detected mutants was 1.49, which was 1.33-fold higher than the average $-\log_2(\text{FC})$ of down-regulated lipid species (Fig. 8b, d). TG, PC, PE, LPC, PS, LPE, and PI were the major lipid classes showing differential expression. Each of these lipid classes contained > 8 DELS, and the total lipid species involved accounted for 90.55% of all DELS (Fig. 8b, c). TG, LPC, LPE, and PI were mainly up-regulated; PE and PS were mainly down-regulated; PC was up-/down-regulated, and the average $\log_2(\text{FC})$ was ~ 0.233 (Fig. 8b, d). Additionally, the differentially expressed lipid classes mainly belonged to two major categories, glycerides and glycerophospholipids.

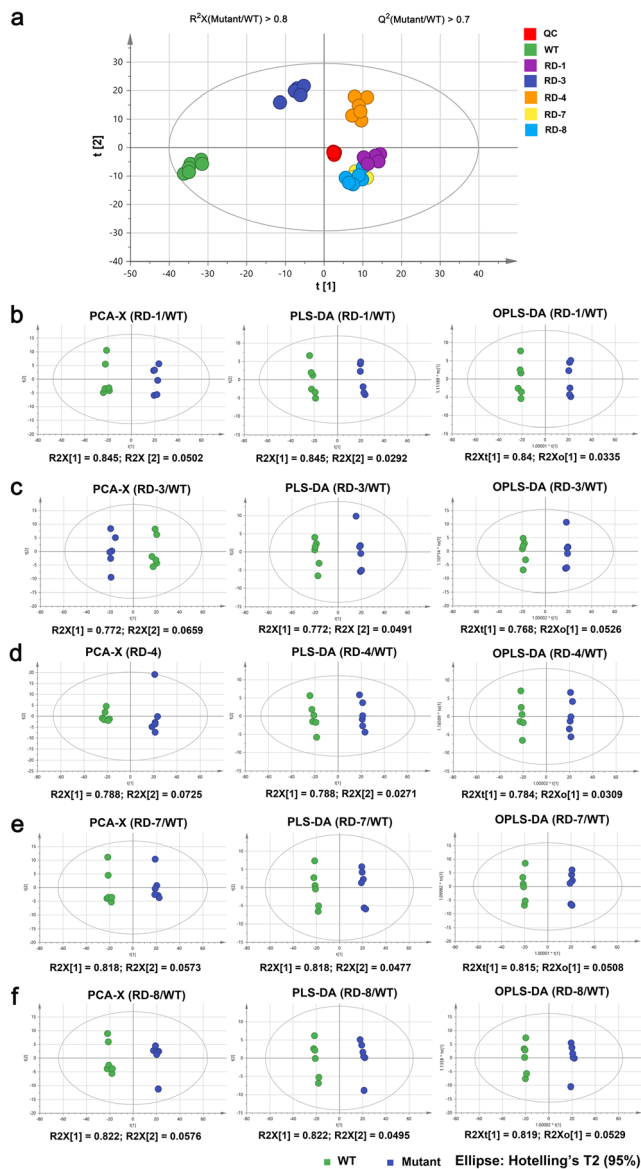


Fig. 7 Distinction of different groups of samples by PCA, PLS-DA, and OPLS-DA models. **a** Principal component analysis of five QC samples, six wild-type strain samples, and 30 mutant samples based on the entire lipidome data. Two main composite variables ($t[1]$ and $t[2]$) were used to reflect information for the original variables. The PCA model parameters R^2X (mutant/control) and Q^2 represent the model interpretation rate and model prediction ability, respectively, and were obtained by 7-fold cross-validation. The relationship between lipid species intensity and groups (mutant/wild-type strain) was fitted using the PCA, PLS-DA, and OPLS-DA models. **b–f** The score plots of three models for five randomly selected mutants. The detailed model parameters are shown in supplemental Table S4

Discussion

Generally, mitochondrial respiratory function is only reduced to a certain extent in mitochondrial diseases (Yu et al. 2017). In this study, large SVs of the mitochondrial genome and severely impaired mitochondrial respiratory function in *S. cerevisiae* essentially reflect the limiting state in human

cells in many mitochondrial diseases. In terms of fate determination, mitochondria play different roles in *S. cerevisiae* and human cells. When mitochondrial respiratory function is severely impaired, *S. cerevisiae* cells can sustain low-rate activity through anaerobic respiration, while most human cells are inactivated (Guo et al. 2019a). However, severely impaired mitochondrial function leads to energy shortage and abnormal mitochondrial components, which block biochemical reactions in *S. cerevisiae* mitochondrial respiration-deficient mutants. These cascade reactions are consistent between *S. cerevisiae* cells in this study and mammalian cells with decreased mitochondrial function. Therefore, the *S. cerevisiae* respiration-deficient mutant selected for this study is a suitable model for human cells in the mitochondrial disease state, demonstrating the high reference value of this study.

The frequency of mtDNA mutations is much higher than that of nuclear DNA (Guo et al. 2019a; Lynch et al. 2008). This characteristic makes it relatively easy to obtain stable *S. cerevisiae* mitochondrial mutants by mutagenesis and directed screening. To study mitochondrial function, *S. cerevisiae* respiration-deficient mutants were obtained by HIB irradiation mutagenesis in our previous study (Guo et al. 2019a). However, HIB irradiation mutagenesis inevitably and randomly led to mitochondrial dysfunction-unrelated mutations in the nuclear genome, interfering with the study on the effects of mitochondrial dysfunction. Thus, this study adopted the following strategies to eliminate interference from the mitochondrial dysfunction-unrelated nuclear genome mutations. First, population studies were conducted based on a mitochondrial respiratory-deficient mutant group; the co-occurrence frequency was used to determine whether any phenotypic or molecular change was caused by a loss of mitochondrial function, as mitochondrial mutation is common to the whole group and mutation in the nuclear genome is typically individual. The second was to use whole-genome sequencing to obtain a clear population genetic background. Determining the threshold of co-occurrence frequency requires a clear genetic background of the population, and whether there are nuclear genome mutations that can interfere with the focused scientific questions under study can be quantitatively judged. In the present study, all of the nuclear genome mutations, and thus potentially affected genes and metabolic pathways, showed a co-occurrence frequency of ≤ 3 in the investigated mutant population. Therefore, DEGs with a co-occurrence frequency of ≥ 4 and ≥ 5 were selected for their respective KEGG enrichment analysis to identify the metabolic pathway significantly affected by mitochondrial dysfunction at the transcriptional level. The enrichment results for DEGs ≥ 4 and ≥ 5 were similar, and lipid metabolism was the most significantly enriched KEGG term. Any identified DEG related to lipid metabolism showed the same up-/down-regulated pattern among nearly all eight mutants. Any

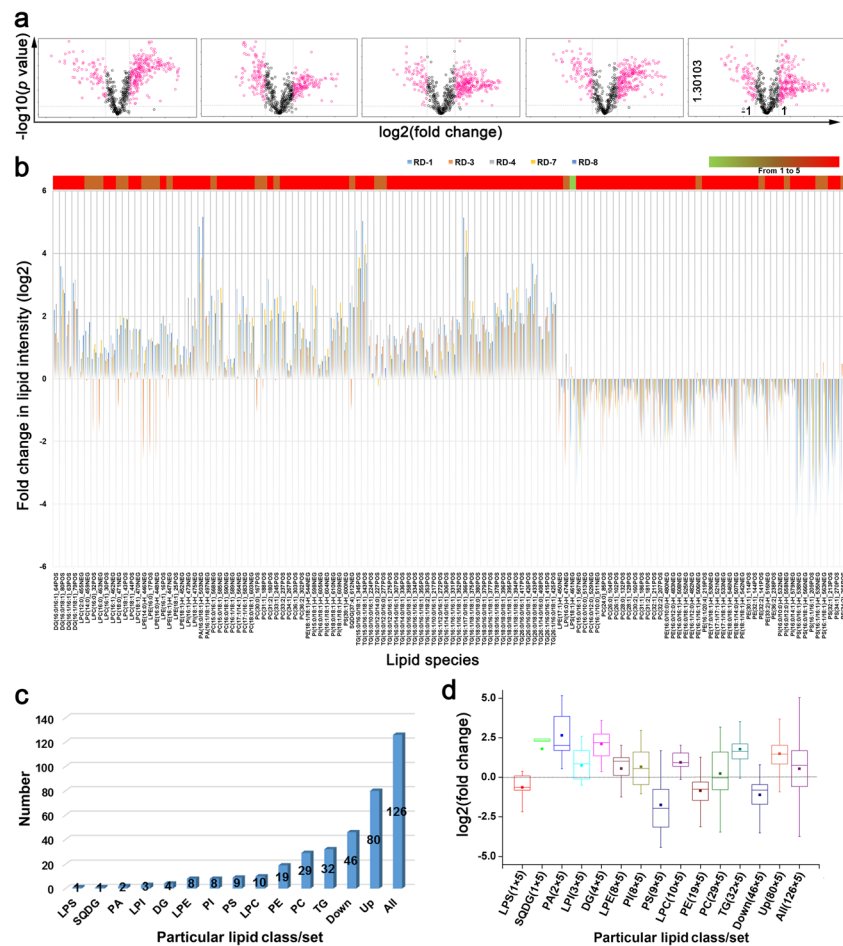


Fig. 8 Expression pattern of DELS identified by UHPLC-ITMS in the five randomly selected mutants. **a** Volcano plots highlighting the lipid species with $p < 0.05$, $FC > 2$ or < 0.5 in mutants. **b** DELS after considering the VIP value in the OPLS-DA model, in which those with $VIP \geq 1$, p value ≥ 0.05 , and $FC \leq 1.5$ and ≥ 0.68 were filtered out; a heatmap corresponding to the lipid species was used to indicate the frequency of mutants with the same up- or down-regulation pattern. Overall, all DELS showed the same up-/down-regulated pattern among nearly all mutants

identified DELS also exhibited a common up-/down-regulation pattern among nearly all examined mutants. This illustrates the rationality of our threshold selection. Additionally, genomic analysis revealed that only a lipid metabolism-related pathway was likely to be affected by the nuclear genome mutations in the RD-1 strain. Therefore, changes in lipid species that co-existed in nearly all investigated mutants were only attributed to mitochondrial dysfunction in this study.

The investigation on mitochondrial function in this study was based on a multi-omics analysis, making the results more detailed and rigorous. Genomic analysis revealed the properties of the study material and provided a clear genetic background. Significant SVs in the mitochondrial genome were common to the entire *S. cerevisiae* mutant population investigated in this study. The nuclear genome of each mutant showed an average of only 14 mutation sites, and the average number of genes potentially affected by the mutations was 11.

examined. **c** Distribution of DELS in different classes (or sets). **d** Statistical results for FC in expression intensity of DELS included in different classes (or sets); the content in the brackets following lipid class (or set) name represents the number of the values involved in the statistics, which were obtained by the number of identified DELS \times the number of investigated mutants. Square filled with a specific color indicated the average value

Additionally, nuclear genome mutations were unique to each other with very few intersections. This genetic background determined that the interference from the mitochondrial dysfunction-unrelated nuclear genome mutations can be eliminated by setting high thresholds of co-occurrence frequency of differentially expressed molecules among mutant population. Therefore, the mitochondrial respiration-deficient mutant population used in this study is a suitable model for conducting mitochondrial function studies. Gene transcription is an important process for producing phenotypic characteristics. In this study, we quantitatively compared the extent to which each metabolic change was affected by mitochondrial dysfunction at the transcriptional level, and lipid metabolism was considered the most significantly enriched pathway. However, it is difficult to accurately characterize and quantify changes in gene products corresponding to genetic variation only based on transcriptional results. The changes are

determined by the complex cellular metabolic network (Logue and Morrison 2012; Volterra et al. 2014). In this study, the metabolisms of most lipid classes interact with each other. The analysis on glycerophospholipid metabolism network showed that the change pattern of a glycerophospholipid species is a comprehensive effect caused by the potential changes both in incoming and outgoing, as well as dense crosstalk from various other metabolites in the metabolic network. The fatty acid synthesis and degradation pathways were simultaneously affected both by the up- and down-regulated DEGs. This suggests that, in this study, most of the DELS were more inclined to be an anfractuous comprehensive effect caused by the relevant DEGs. Meanwhile, transcription is only one process involved in gene product formation. The relationship between the number of transcripts and abundances of gene products is not linear and is also affected by translation, biological enzyme catalysis, and many other biological processes. Therefore, metabolomic analysis was performed based on transcriptomic analysis, which further accurately and quantitatively described changes in gene products caused by genomic changes. Significant changes in lipid species in all investigated mutants confirmed the predictions of transcriptomic analysis. Additionally, the DELS showed the same up-/down-regulated patterns among nearly all examined mutants, which was consistent with the results of transcriptomic analysis. Overall, the genomic, transcriptomic, and metabolomic results were mutually causal and validated.

Mitochondria are one of the major organelles directly involved in lipid metabolism. Fatty acids are the simplest type of fat and are components of many complex lipid molecules. In the presence of intact mitochondrial function, acetyl-CoA produced in mitochondria is an important carbon source for fatty acid synthesis (Moreau et al. 2006; Yang et al. 2019). Transport of acetyl-CoA to the outside of mitochondria depends on the “citrate pyruvate cycle” that occurs in mitochondria (Mishra et al. 2016; Yang et al. 2019). By continuously condensing acetyl-CoA to the carboxy terminus, the carbon chain of palmitic acid or other saturated fatty acids can be prolonged in mitochondria (Van Vranken et al. 2018). In addition, the beta oxidation of fatty acids is mostly completed in mitochondria. Fatty acyl-CoA produced by the activation of fatty acids is transported to mitochondria, which is oxidatively decomposed to produce energy, carbon dioxide, and water (Adeva-Andany et al. 2019). Additionally, changes in the mitochondrial energy supply, various signalling pathways related to mitochondria, and mitochondrial metabolite-mediated epigenetic modifications certainly affect numerous cellular pathways, including lipid metabolism. Although mitochondria play an important role in lipid metabolism, few quantitative indicators have been identified for measuring the relative and absolute effects of mitochondria on lipid metabolism. This study demonstrated that the most enriched KEGG term of the DEGs was lipid metabolism when mitochondrial

function was deficient. Further, the results of lipidomic analysis quantified the effect of mitochondrial dysfunction on lipid metabolism. In detail, the DELS accounted for more than 20% of the total lipid species identified; the average $\log_2(\text{FC})$ of each DELS in each mutant was 0.54. For the entire examined mutant population, the number and average $|\log_2(\text{FC})|$ of the up-regulated lipid species were 1.74- and 1.33-fold higher than those of down-regulated lipid species, respectively. The lipid class with the most obvious variance was TG, which appeared to be only up-regulated. TG is an important fat for energy storage and energy supply in *S. cerevisiae* cells. This conclusion is consistent with previous findings showing that decreased mitochondrial number or function will increase the risk of diseases such as atherosclerosis and fatty liver (Peng et al. 2019; Wieckowski et al. 2019).

PE and PC, the most abundant phospholipid classes in the plasma membrane (Patel and Witt 2017; van der Veen et al. 2017), mainly presented an obvious change in relative proportion. In particular, PE species showed an obvious decrease in content among the entire mitochondrial respiration-deficient mutant population. This phenomenon is consistent with the fact that PE synthesis via the PS decarboxylase (PSD) pathway or the acylation of LPE is closely related to mitochondria (Horvath and Daum 2013; Vance 2018). The PSD pathway occurs in mitochondria; in several types of cultured cells, more than 80% of PE appears to be derived from the PSD pathway (Vance 2018). The production of PE by the acylation of LPE is active in yeasts, in which the majority of LPE acyltransferase activity is localized to the mitochondria-associated membranes (Vance 2018). For PC species, 15 of them were up-regulated and 14 of them were down-regulated. This change pattern for PC species was common among the entire investigated population, and the average $\log_2(\text{FC})$ was ~ 0.233 . Thus, the ratio of PE and PC decreased. Therefore, mitochondrial dysfunction corresponded to an increased fat content and a decreased ratio between PE and PC. Previous data showing that changes in the PC and/or PE content of various tissues are implicated in metabolic disorders such as atherosclerosis, insulin resistance, obesity, and cancer (Fahrman et al. 2016; Patel and Witt 2017; van der Veen et al. 2017, 2019). At the cellular level, phospholipids in biological membranes typically play a key role in cellular biological function and membrane molecular organization (Arashiki and Takakuwa 2017; Pennington et al. 2019; Renne and de Kroon 2018). For example, PE, a phospholipid class showing an obvious down-regulation in our study model, has attracted much interest due to its wide-ranging effects on cells. In the mammalian cell model, PE has been confirmed to be involved in signal transduction, such as activation of many cell surface signalling proteins and the initiation of autophagy process (Patel and Witt 2017; Vance 2018). The other remarkable activities of

PE include: assisting in the folding of certain membrane proteins (Patel and Witt 2017); promoting membrane curvature, enhancing the membrane fusion, and regulating the membrane fluidity (Dawaliby et al. 2016; Vance 2018). It is also required for the activity of several of the respiratory complexes (Patel and Witt 2017). In the *S. cerevisiae* cell model, studies revealed that the lack of PE can result in a failure of the permease targeting to plasma membrane (Opekarova et al. 2002). PE made in the inner mitochondrial membrane is also essential for yeast cytochrome bc₁ complex function (Calzada et al. 2019).

In the present study, multi-omics analysis was combined with the investigation on co-occurrence frequency of mutations and differentially expressed molecules among the entire investigated mutant population, which were demonstrated to be effective for eliminating interference from the mitochondrial dysfunction-unrelated nuclear genome mutations. In conclusion, the similar up-/down-regulated change patterns of the identified lipid metabolism-related DEGs and DELS among the nearly all examined mutants can be conservatively attributed to population commonality (large deletions in the mitochondrial genome and remarkable mitochondrial dysfunction) but not individual characteristics (unique mitochondrial dysfunction-unrelated nuclear genome mutations in each mutant). Based on this, lipid metabolism was revealed as one of the most vulnerable cellular pathways affected by mitochondrial dysfunction. The change in the spectrum of lipid species attributed to mitochondrial dysfunction was quantitatively mapped. The affected lipids have characteristics of many kinds and deep degree. Specifically, mitochondrial dysfunction mainly up-regulated energy storage-related fat and decreased ratio between PE and PC. Additionally, the established strategies in this study provides an important reference for high-throughput mitochondrial DNA mutation-related functional studies at the population level. Particularly, the co-occurrence frequency was consistent throughout genomic, transcriptomic, and metabolomic analyses.

Acknowledgments We thank the colleagues at HIRFL for providing high-quality carbon ion beam irradiation.

Human and animal rights This article does not contain any studies with human participants or animals performed by any of the authors.

Funding information This work was supported by the National Natural Science Foundation of China (No. 11975284 and No. 11905265), the Joint project of the Chinese Academy of Sciences and the Industrial Technology Research Institute (CAS-ITRI 2019012), and the Science and Technology Program of Lanzhou, China (2019-1-39).

Compliance with ethical standards

Conflict of interest The authors declare that they have no conflicts of interest.

References

- Adeva-Andany MM, Carneiro-Freire N, Seco-Filgueira M, Fernandez-Fernandez C, Mourino-Bayolo D (2019) Mitochondrial beta-oxidation of saturated fatty acids in humans. *Mitochondrion* 46: 73–90. <https://doi.org/10.1016/j.mito.2018.02.009>
- Arashiki N, Takakuwa Y (2017) Maintenance and regulation of asymmetric phospholipid distribution in human erythrocyte membranes: implications for erythrocyte functions. *Curr Opin Hematol* 24(3): 167–172. <https://doi.org/10.1097/moh.0000000000000326>
- Bacman SR, Kauppila JHK, Pereira CV, Nissanka N, Miranda M, Pinto M, Williams SL, Larsson NG, Stewart JB, Moraes CT (2018) MitoTALEN reduces mutant mtDNA load and restores tRNA(Ala) levels in a mouse model of heteroplasmic mtDNA mutation. *Nat Med* 24(11):1696–1700. <https://doi.org/10.1038/s41591-018-0166-8>
- Benador IY, Veliova M, Mahdavi K, Petcherski A, Wikstrom JD, Assali EA, Acin-Perez R, Shum M, Oliveira MF, Cinti S, Sztalryd C, Barshop WD, Wohlschlegel JA, Corkey BE, Liesa M, Shirihai OS (2018) Mitochondria bound to lipid droplets have unique bioenergetics, composition, and dynamics that support lipid droplet expansion. *Cell Metab* 27(4):869–885. <https://doi.org/10.1016/j.cmet.2018.03.003>
- Calvo SE, Clauser KR, Mootha VK (2016) MitoCarta2.0: an updated inventory of mammalian mitochondrial proteins. *Nucleic Acids Res* 44(D1):D1251–D1257. <https://doi.org/10.1093/nar/gkv1003>
- Calzada E, Avery E, Sam PN, Modak A, Wang CY, McCaffery JM, Han XL, Alder NN, Claypool SM (2019) Phosphatidylethanolamine made in the inner mitochondrial membrane is essential for yeast cytochrome bc(1) complex function. *Nat Commun* 10:17–17. <https://doi.org/10.1038/s41467-019-09425-1>
- Chouchani ET, Pell VR, Gaude E, Aksentjevic D, Sundier SY, Robb EL, Logan A, Nadtochiy SM, Ord ENJ, Smith AC, Eyassu F, Shirley R, Hu CH, Dare AJ, James AM, Rogatti S, Hartley RC, Eaton S, Costa ASH, Brookes PS, Davidson SM, Duchon MR, Saeb-Parsy K, Shattock MJ, Robinson AJ, Work LM, Frezza C, Krieg T, Murphy MP (2014) Ischaemic accumulation of succinate controls reperfusion injury through mitochondrial ROS. *Nature* 515(7527):431–435. <https://doi.org/10.1038/nature13909>
- Dawaliby R, Trubbia C, Delporte C, Noyon C, Ruyschaert JM, Van Antwerpen P, Govaerts C (2016) Phosphatidylethanolamine is a key regulator of membrane fluidity in eukaryotic cells. *J Biol Chem* 291(7):3658–3667. <https://doi.org/10.1074/jbc.M115.706523>
- Dobson AW, Xu Y, Kelley MR, LeDoux SP, Wilson GL (2000) Enhanced mitochondrial DNA repair and cellular survival after oxidative stress by targeting the human 8-oxoguanine glycosylase repair enzyme to mitochondria. *J Biol Chem* 275(48):37518–37523. <https://doi.org/10.1074/jbc.M000831200>
- Du Y, Li W, Yu L, Chen G, Liu Q, Luo S, Shu Q, Zhou L (2014) Mutagenic effects of carbon-ion irradiation on dry *Arabidopsis thaliana* seeds. *Mutat Res-Gen Tox En* 759(1):28–36. <https://doi.org/10.1016/j.mrgentox.2013.07.018>
- Du Y, Luo S, Li X, Yang J, Cui T, Li W, Yu L, Feng H, Chen Y, Mu J (2017) Identification of substitutions and small insertion-deletions induced by carbon-ion beam irradiation in *Arabidopsis thaliana*. *Front Plant Sci* 8:1851. <https://doi.org/10.3389/fpls.2017.01851>
- Ejsing CS, Sampaio JL, Surendranath V, Duchoslav E, Ekroos K, Klemm RW, Simons K, Shevchenko A (2009) Global analysis of the yeast lipidome by quantitative shotgun mass spectrometry. *Proc Natl Acad Sci U S A* 106(7):2136–2141. <https://doi.org/10.1073/pnas.0811700106>
- Fahrman JF, Grapov D, DeFelice BC, Taylor S, Kim K, Kelly K, Wikoff WR, Pass H, Rom WN, Fiehn O, Miyamoto S (2016) Serum phosphatidylethanolamine levels distinguish benign from malignant

- solitary pulmonary nodules and represent a potential diagnostic biomarker for lung cancer. *Cancer Biomark* 16(4):609–617. <https://doi.org/10.3233/cbm-160602>
- Feng H, Yu Z, Chu PK (2006) Ion implantation of organisms. *Mater Sci Eng R* 54(3):49–120. <https://doi.org/10.1016/j.mser.2006.11.001>
- Frazier AE, Thorburn DR, Compton AG (2019) Mitochondrial energy generation disorders: genes, mechanisms, and clues to pathology. *J Biol Chem* 294(14):5386–5395. <https://doi.org/10.1074/jbc.R117.809194>
- Gammage PA, Viscomi C, Simard ML, Costa ASH, Gaude E, Powell CA, Van Haute L, McCann B, Rebelo-Guiomar P, Cerutti R, Zhang L, Rebar EJ, Zeviani M, Frezza C, Stewart JB, Minczuk M (2018) Genome editing in mitochondria corrects a pathogenic mtDNA mutation in vivo. *Nat Med* 24(11):1691–1695. <https://doi.org/10.1038/s41591-018-0165-9>
- Guo XP, Zhang MM, Gao Y, Cao GZ, Yang Y, Lu D, Li WJ (2019a) A genome-wide view of mutations in respiration-deficient mutants of *Saccharomyces cerevisiae* selected following carbon ion beam irradiation. *Appl Microbiol Biotechnol* 103(4):1851–1864. <https://doi.org/10.1007/s00253-019-09626-0>
- Guo XP, Zhang MM, Liu RY, Gao Y, Yang Y, Li WJ, Lu D (2019b) Repair characteristics and time-dependent effects in *Saccharomyces cerevisiae* cells after X-ray irradiation. *World J Microbiol Biotechnol* 35(1):15–15. <https://doi.org/10.1007/s11274-018-2566-9>
- Gureev AP, Shafarostova EA, Popov VN (2019) Regulation of mitochondrial biogenesis as a way for active longevity: interaction between the Nrf2 and PGC-1 alpha signaling pathways. *Front Genet* 10:12. <https://doi.org/10.3389/fgene.2019.00435>
- Hirose M, Schilf P, Gupta Y, Wright MN, Jöhren O, Wagner AE, Sina C, Ziegler A, Ristow M, Ibrahim SM (2016) Lifespan effects of mitochondrial mutations. *Nature* 540(7633):E13–E14. <https://doi.org/10.1038/nature20778>
- Horvath SE, Daum G (2013) Lipids of mitochondria. *Prog Lipid Res* 52(4):590–614. <https://doi.org/10.1016/j.plipres.2013.07.002>
- Krzywinski M, Schein J, Birol I, Connors J, Gascoyne R, Horsman D, Jones SJ, Marra MA (2009) Circos: An information aesthetic for comparative genomics. *Genome Res* 19(9):1639–1645. <https://doi.org/10.1101/gr.092759.109>
- Li X, Wang J, Tan Z, Ma L, Lu D, Li W, Wang J (2018) Cd resistant characterization of mutant strain irradiated by carbon-ion beam. *J Hazard Mater* 353:1–8. <https://doi.org/10.1016/j.jhazmat.2018.03.036>
- Luo SW, Zhou LB, Li WJ, Du Y, Yu LX, Feng H, Mu JH, Chen YZ (2016) Mutagenic effects of carbon ion beam irradiations on dry *Lotus japonicus* seeds. *Nucl Instrum Meth B* 383:123–128. <https://doi.org/10.1016/j.nimb.2016.06.021>
- Logue JS, Morrison DK (2012) Complexity in the signaling network: insights from the use of targeted inhibitors in cancer therapy. *Genes Dev* 26(7):641–650. <https://doi.org/10.1101/gad.186965.112>
- Lozoya OA, Martinez-Reyes I, Wang TY, Grenet D, Bushel P, Li JY, Chandel N, Woychik RP, Santos JH (2018) Mitochondrial nicotinamide adenine dinucleotide reduced (NADH) oxidation links the tricarboxylic acid (TCA) cycle with methionine metabolism and nuclear DNA methylation. *PLoS Biol* 16(4):23. <https://doi.org/10.1371/journal.pbio.2005707>
- Lynch M, Sung W, Morris K, Coffey N, Landry CR, Dopman EB, Dickinson WJ, Okamoto K, Kulkarni S, Hartl DL, Thomas WK (2008) A genome-wide view of the spectrum of spontaneous mutations in yeast. *Proc Natl Acad Sci U S A* 105(27):9272–9277. <https://doi.org/10.1073/pnas.0803466105>
- Mao WJ, Liu ZZ, Zhu H, Zhu RR, Sun XY, Yao SD, Wang SL (2009) Selection of the respiration deficiency mutant yeast irradiated by laser and optimization of the fermentation condition. *J Rad Res Rad Proc* 27(1):1–4
- Matilainen O, Quiros PM, Auwerx J (2017) Mitochondria and epigenetics crosstalk in homeostasis and stress. *Trends Cell Biol* 27(6):453–463. <https://doi.org/10.1016/j.tcb.2017.02.004>
- Mayorga L, Salassa BN, Marzese DM, Loos MA, Eiroa HD, Lubieniecki F, Samartino CG, Romano PS, Roque M (2019) Mitochondrial stress triggers a pro-survival response through epigenetic modifications of nuclear DNA. *Cell Mol Life Sci* 76(7):1397–1417. <https://doi.org/10.1007/s00018-019-03008-5>
- Mishra P, Park GY, Lakshmanan M, Lee HS, Lee H, Chang MW, Ching CB, Ahn J, Lee DY (2016) Genome-scale metabolic modeling and in silico analysis of lipid accumulating yeast *Candida tropicalis* for dicarboxylic acid production. *Biotechnol Bioeng* 113(9):1993–2004. <https://doi.org/10.1002/bit.25955>
- Moreau K, Dizin E, Ray H, Luquin C, Lefai E, Foufelle F, Billaud M, Lenoir GM, Dalla Venezia N (2006) BRCA1 affects lipid synthesis through its interaction with acetyl-CoA carboxylase. *J Biol Chem* 281(6):3172–3181. <https://doi.org/10.1074/jbc.M504652200>
- Niemann J, Johne C, Schroder S, Koch F, Ibrahim SM, Schultz J, Tiedge M, Baltrusch S (2017) An mtDNA mutation accelerates liver aging by interfering with the ROS response and mitochondrial life cycle. *Free Radic Biol Med* 102:174–187. <https://doi.org/10.1016/j.freeradbiomed.2016.11.035>
- Opekarova M, Robl I, Tanner W (2002) Phosphatidyl ethanolamine is essential for targeting the arginine transporter Can1p to the plasma membrane of yeast. *Biochim Biophys Acta-Biomembr* 1564(1):9–13. [https://doi.org/10.1016/s0005-2736\(02\)00455-8](https://doi.org/10.1016/s0005-2736(02)00455-8)
- Patel D, Witt SN (2017) Ethanolamine and phosphatidylethanolamine: partners in health and disease. *Oxidative Med Cell Longev*:1–18. <https://doi.org/10.1155/2017/4829180>
- Peng WX, Cai GD, Xia YP, Chen JN, Wu P, Wang Z, Li GH, Wei DH (2019) Mitochondrial dysfunction in atherosclerosis. *DNA Cell Biol* 38(7):597–606. <https://doi.org/10.1089/dna.2018.4552>
- Pennington ER, Funai K, Brown DA, Shaikh SR (2019) The role of cardiolipin concentration and acyl chain composition on mitochondrial inner membrane molecular organization and function. *Biochim Biophys Acta Mol Cell Biol Lipids* 1864(7):1039–1052. <https://doi.org/10.1016/j.bbalip.2019.03.012>
- Renne MF, de Kroon A (2018) The role of phospholipid molecular species in determining the physical properties of yeast membranes. *FEBS Lett* 592(8):1330–1345. <https://doi.org/10.1002/1873-3468.12944>
- Ryzhkova AI, Sazonova MA, Sinyov VV, Galitsyna EV, Chicheva MM, Melnichenko AA, Grechko AV, Postnov AY, Orekhov AN, Shkurat TP (2018) Mitochondrial diseases caused by mtDNA mutations: a mini-review. *Therap Clin Risk Manag* 14:1933–1942. <https://doi.org/10.2147/tcrm.s154863>
- Schell JC, Wisidagama DR, Bensard C, Zhao HL, Wei P, Tanner J, Flores A, Mohlman J, Sorensen LK, Earl CS, Olson KA, Miao R, Waller TC, Delker D, Kanth P, Jiang L, DeBerardinis RJ, Bronner MP, Li DY, Cox JE, Christofk HR, Lowry WE, Thummel CS, Rutter J (2017) Control of intestinal stem cell function and proliferation by mitochondrial pyruvate metabolism. *Nat Cell Biol* 19(9):1027–1036. <https://doi.org/10.1038/ncb3593>
- Sickmann A, Reinders J, Wagner Y, Joppich C, Zahedi R, Meyer HE, Schonfisch B, Perschil I, Chacinska A, Guiard B, Rehling P, Pfanner N, Meisinger C (2003) The proteome of *Saccharomyces cerevisiae* mitochondria. *Proc Natl Acad Sci U S A* 100(23):13207–13212. <https://doi.org/10.1073/pnas.213585100>
- Solieri L (2010) Mitochondrial inheritance in budding yeasts: towards an integrated understanding. *Trends Microbiol* 18(11):521–530. <https://doi.org/10.1016/j.tim.2010.08.001>
- Spangenberg L, Grana M, Mansilla S, Martinez J, Tapie A, Greif G, Montano N, Vaglio A, Guecaimburu R, Robello C, Castro L, Quijano C, Raggio V, Naya H (2019) Deep sequencing discovery of causal mtDNA mutations in a patient with unspecific neurological

- disease. *Mitochondrion* 46:337–344. <https://doi.org/10.1016/j.mito.2018.09.004>
- St John JC (2016) Mitochondrial DNA copy number and replication in reprogramming and differentiation. *Semin Cell Dev Biol* 52:93–101. <https://doi.org/10.1016/j.semcdb.2016.01.028>
- Sun C, Liu XX, Di CX, Wang ZH, Mi XQ, Liu Y, Zhao QY, Mao AH, Chen WQ, Gan L, Zhang H (2017) MitoQ regulates autophagy by inducing a pseudo-mitochondrial membrane potential. *Autophagy* 13(4):730–738. <https://doi.org/10.1080/15548627.2017.1280219>
- van der Veen JN, Kennelly JP, Wan S, Vance JE, Vance DE, Jacobs RL (2017) The critical role of phosphatidylcholine and phosphatidylethanolamine metabolism in health and disease. *Biochim Biophys Acta-Biomembr* 1859(9):1558–1572. <https://doi.org/10.1016/j.bbmem.2017.04.006>
- van der Veen JN, Lingrell S, McCloskey N, LeBlond ND, Galleguillos D, Zhao YY, Curtis JM, Sipione S, Fullerton MD, Vance DE, Jacobs RL (2019) A role for phosphatidylcholine and phosphatidylethanolamine in hepatic insulin signaling. *FASEB J* 33(4):5045–5057. <https://doi.org/10.1096/fj.201802117R>
- Vance JE (2018) Historical perspective: phosphatidylserine and phosphatidylethanolamine from the 1800s to the present. *J Lipid Res* 59(6):923–944. <https://doi.org/10.1194/jlr.R084004>
- Van Houten B, Hunter SE, Meyer JN (2016) Mitochondrial DNA damage induced autophagy, cell death, and disease. *Front Biosci* 21:42–54. <https://doi.org/10.2741/4375>
- Van Vranken JG, Nowinski SM, Clowers KJ, Jeong MY, Ouyang YY, Berg JA, Gygi JP, Gygi SP, Winge DR, Rutter J (2018) ACP acylation is an acetyl-CoA-dependent modification required for electron transport chain assembly. *Mol Cell* 71(4):567–580. <https://doi.org/10.1016/j.molcel.2018.06.039>
- Volterra A, Liaudet N, Savtchouk I (2014) Astrocyte Ca²⁺ signalling: an unexpected complexity. *Nat Rev Neurosci* 15(5):327–335. <https://doi.org/10.1038/nrn3725>
- Wieckowski M, Simoes I, Karkucinska-Wieckowska A, Janikiewicz J, Schmitt S, Szymanska S, Pronicki M, Dobrzyn P, Zischka H, Dobrzyn A, Oliveira P (2019) Mitochondrial dysfunction in non-alcoholic fatty liver disease. *Eur J Clin Invest* 49:18–19
- Wu JM, Mao XZ, Cai T, Luo JC, Wei LP (2006) KOBAS server: a web-based platform for automated annotation and pathway identification. *Nucleic Acids Res* 34:W720–W724. <https://doi.org/10.1093/nar/gkl167>
- Yan CJ, Duanmu XY, Zeng L, Liu B, Song ZY (2019) Mitochondrial DNA: distribution, mutations, and elimination. *Cells* 8(4):15. <https://doi.org/10.3390/cells8040379>
- Yang JH, Li SQ, Khan MAK, Garre V, Vongsangnak W, Song YD (2019) Increased lipid accumulation in *Mucor circinelloides* by overexpression of mitochondrial citrate transporter genes. *Ind Eng Chem Res* 58(6):2125–2134. <https://doi.org/10.1021/acs.iecr.8b05564>
- Yu EPK, Reinhold J, Yu HX, Starks L, Uryga AK, Foote K, Finigan A, Figg N, Pung YF, Logan A, Murphy MP, Bennett M (2017) Mitochondrial respiration is reduced in atherosclerosis, promoting necrotic core formation and reducing relative fibrous cap thickness. *Arterioscler Thromb Vasc Biol* 37(12):2322–2332. <https://doi.org/10.1161/atvbaha.117.310042>
- Zhang H, Lu D, Li X, Feng Y, Cui Q, Song X (2018a) Heavy ion mutagenesis combined with triclosan screening provides a new strategy for improving the arachidonic acid yield in *Mortierella alpina*. *BMC Biotechnol* 18(1):23. <https://doi.org/10.1186/s12896-018-0437-y>
- Zhang MM, Guo XP, Liu RY, Ma L, Gao Y, Lu D, Li WJ (2018b) Lipidomics studies on mitochondrial damage of *Saccharomyces cerevisiae* induced by heavy ion beam radiation. *Chin J Anal Chem* 46(11):1714–1723. [https://doi.org/10.1016/s1872-2040\(18\)61123-5](https://doi.org/10.1016/s1872-2040(18)61123-5)
- Zhao XS, Ren X, Zhu R, Luo ZY, Ren BX (2016) Zinc oxide nanoparticles induce oxidative DNA damage and ROS-triggered mitochondria-mediated apoptosis in zebrafish embryos. *Aquat Toxicol* 180:56–70. <https://doi.org/10.1016/j.aquatox.2016.09.013>

Publisher's note Springer Nature remains neutral with regard to jurisdictional claims in published maps and institutional affiliations.